Dictionary-based Sparse Representation for Resolution Improvement in Laser Voltage Imaging of CMOS Integrated Circuits

T. Berkin Cilingiroglu*, Mahmoud Zangeneh*, Aydan Uyar*, W. Clem Karl*, Janusz Konrad*, Ajay Joshi*,
Bennett B. Goldberg† and M. Selim Unlu*
*Department of Electrical and Computer Engineering †Department of Physics
Boston University, Boston, MA 02215

***Abstract*—The rapid decrease in the dimensions of integrated circuits with a simultaneous increase in component density have introduced resolution challenges for optical failure analysis techniques. Although optical microscopy efforts continue to increase resolution of optical systems through hardware modifications, signal processing methods are essential to complement these efforts to meet the resolution requirements for the nanoscale integrated circuit technologies. In this work, we focus on laser voltage imaging as the optical failure analysis technique and show how an overcomplete dictionary-based sparse representation can improve resolution and localization accuracy. We describe a reconstruction approach based on this sparse representation and validate its performance on simulated data. We achieve an 80% reduction of the localization error.**

I. Introduction

As we scale CMOS transistors into the sub-22 nm regime, the increasing density and smaller feature sizes in integrated circuits (ICs) create resolution challenges for optical failure analysis (FA) techniques. The state-of-the-art backside fault analysis approach is to use aplanatic solid immersion lenses (aSILs) in order to achieve the highest possible numerical aperture (NA) [1]. The optical microscopy efforts for increasing resolution of backside optical FA systems continue through hardware modifications, such as the use of radially polarized light for illumination [2] and the use of apodization masks, but they are not enough to meet the resolution requirements of new ICs. Therefore, there is a need for model-based signal processing approaches to increase resolution. Sparse image reconstruction techniques have been previously used to recover high frequency information that is lost during acquisition process in different imaging domains, such as ultrasound [3], synthetic aperture radar [4], optical microscopy [5] and high NA IC microscopy [6], [7].

Laser voltage imaging (LVI) [8] is a failure analysis technique that maps specific frequencies of operation to physical transistor locations. The IC is probed through the backside, hence the resolution challenges in backside optical analysis techniques also exist in LVI. In this work, our goal is to use dictionary-based sparse reconstruction techniques for spatial resolution improvement of LVI data. When a CMOS transistor is driven with a rectangular pulse, modulations are observed on the reflected light mainly due to change in free-carrier densities underneath gate and drain regions [9]. LVI technique observes modulations at specific frequencies collecting amplitudes of harmonics in frequency domain. In this work, we propose to collect LVI data at multiple harmonics, formulate a dictionary-based sparse representation framework to increase spatial resolution of LVI data and to increase localization accuracy of regions with different modulation behavior. Multiple harmonics LVI data is highly structured both spatially and in frequency domain. Therefore, it is a well-suited application domain for overcomplete dictionary-based sparse image reconstruction. Active regions are mostly composed of rectangular structures with varying width, length and orientation, and these regions are derivable from CAD layouts and design parameters. Additionally, given the applied rectangular pulse, the modulation has a structured frequency domain which can be expressed in terms of Fourier series coefficients of a rectangular pulse. Therefore, 3D overcomplete dictionaries can be predetermined in order to sparsely represent LVI data in space-frequency.

Sparse signal representation through overcomplete dictionaries has been well studied in the image reconstruction literature. Predetermined overcomplete dictionaries, such as a wavelet based dictionary [10], a point and region-based dictionary or a shape-based dictionary [11], have been used to sparsely represent the scene being imaged. Also, application of overcomplete dictionaries for resolution improvement of optical backside images of static IC components has been proposed [7]. Application of such a technique is especially interesting for LVI data because LVI images are sparser and active regions have stronger constraints than static components.

This paper is organized as follows. In Section II, we provide background on the origin of LVI signal, introduce an observation model and explain the details of LVI simulation. The sparse representation framework is presented in Section III with details about the construction of dictionaries in Section III-A. We present experimental results on simulated data in Section IV. In Section V, we provide summary and conclusions.

II. LVI Simulation and Observation Model

The origin of LVI signal can be explained by the absorption and refraction due to free carriers [9]. When a CMOS transistor is driven with a rectangular pulse, it keeps switching

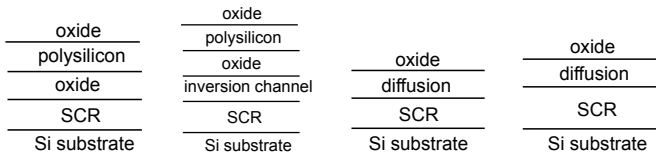

(a) (b) (c) (d)

Fig. 1: Layered structure of the transistor around gate a) cut-off regime b) linear operating regime, and around drain c) cut-off regime d) linear operating regime

between cut-off regime and linear operating regime. The layered structure around gate and drain regions is different for these regimes. In Fig. 1, this layered structure in gate and drain regions is shown for both regimes. The inversion layer is formed with the change in the gate voltage. The refractive index and the absorption coefficient of inversion layer can be calculated using the change in free carrier densities according to equations given in [9]. Besides the inversion layer, there is also a change in the thickness of space charge region (SCR) underneath the gate and drain regions. At a gate voltage of 0 V, the charges in the gate stack result in an initial SCR. When a non-zero voltage is applied to the gate terminal, for voltages below the threshold voltage V_{thr} and a constant doping profile, the SCR thickness can be estimated from the following equation [9]:

$$t_{SCR,initial} = \sqrt{\frac{2\epsilon_0\epsilon_{Si}}{q}(\frac{1}{N_{diff}} + \frac{1}{N_{well}})(V_{bi} - V_G)}, \quad (1)$$

where t_{SCR} is the thickness of the SCR, N_{diff} and N_{well} are the diffusion and well doping concentrations. V_{bi} is the built-in potential [9] and V_G is the voltage applied to the gate of the NFETs. V_G also effects the SCR in the junctions and the following equation can be used to calculate the thickness of the SCR in the junctions [9]:

$$t_{SCR} = t_{SCR,initial} + \sqrt{\frac{2\epsilon_0\epsilon_{Si}}{q}\frac{1}{N_{well}}|V_G|}, \quad (2)$$

where $t_{SCR,initial}$ is the initial SCR thickness when the gate voltage is 0 calculated by Eq. 1. After the threshold voltage is reached, the SCR thickness stays constant and does not increase any further. These changes in the layered structure over time result in changes in the reflected light over time. LVI measurements observe these changes with specific frequencies in the reflected light. The total reflected light can be expressed as $R(x, y, t) = R_0(x, y) + \Delta R(x, y, t)$, where $R_0(x, y)$ is the reflection from the static parts and $\Delta R(x, y, t)$ is the modulated part of the reflected light coming from the active regions. We have used generalized Fresnel reflection coefficients for multi-layered media in order to calculate simulated modulations, $\Delta R(x, y, t)$. The amplitude of the modulated light is taken as the difference of reflected light from transistor in cut-off regime shown in Figs. 1(a), 1(c) and the reflected light from the transistor in linear operating regime shown in Figs. 1(b), 1(d).

When we approximate the blur in the optical system with a linear convolutional model, the blurry and noisy modulations in space and time can be expressed as:

$$\tau^j(x, y, t) = h^j(x, y) * m(x, y, t) + e^j(x, y, t), \quad (3)$$

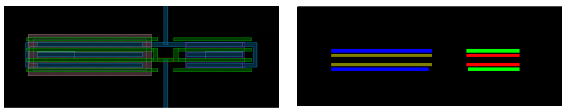

(a) (b)

Fig. 2: (a) CAD layout of an inverter and (b) Active regions of the inverter, red: n-gate, dark green: p-gate, light green: n-drain, blue: p-drain

where $m(x, y, t)$ is the underlying modulation corresponding to $\Delta R(x, y, t)$, $h^j(x, y)$ is the PSF of the high NA imaging system illuminated by linearly polarized input light with polarization direction j and $e^j(x, y, t)$ is the noise in the system. The noise can be modeled as an additive Gaussian noise whose variance scales with the total reflected light. According to experimental data $\Delta R/R_0$ is around 600 parts per million [9]. LVI measures the modulation in the frequency domain. The complex valued temporal harmonics can be expressed as:

$$\mathbf{d}_l^j(x, y) = \frac{1}{T}\int_{<T>} \tau^j(x, y, t)e^{-ilw_0t}\, dt, \quad (4)$$

where l indicates the harmonic number, T is the period of the periodic modulation and w_0 is the fundamental frequency. Then, the observed harmonics LVI data can be collected in vector $\mathbf{d}^j$ whose amplitude and phase can be expressed as $|\mathbf{d}^j|$ and $\angle\mathbf{d}^j$, respectively. In space-frequency, we represent the fourier series coefficients of the underlying modulation $m(x, y, t)$ in terms of an overcomplete 3D space-frequency dictionary. The details of this sparse representation and the reconstruction framework are explained in the next section.

III. Dictionary-based Sparse Representation Framework for Multiple-Harmonics LVI

A. Construction of Dictionaries

Spatially, the dictionaries are constructed by the procedure proposed in [7]. The spatial regions, where the modulations are observed, are rectangular and consist of horizontal and vertical lines of various, pre-defined widths and lengths. These regions can be obtained from the CAD layouts. Spatially, all possible locations of different-size rectangles are included in the dictionary. Fig. 2(a) shows an example of CAD layout for an inverter. Fig.2(b) shows a picture of the support of the gate and drain regions where the modulations are observed. We also need to include all possible frequency signatures of the modulations. The voltage applied to gate is a square wave. Therefore, the modulations in time can be approximated as a rectangular pulse where the rise time and the fall time are much smaller than the pulse width. Depending on the circuit element of interest, the modulations will have the same period as the applied voltage or the period of the modulations will be multiples of the period of the applied voltage. Additionally, depending on the circuit element, the modulations can be in phase with the applied voltage or there might be a time shift. All possible periods and all possible time shifts are also included in the dictionary. The Fourier series coefficients of all possible rectangular pulses are used to determine the third dimension of the dictionary elements. Then, each column of the overcomplete dictionary is the vectorized version of a 3D

block where a region with fixed width and height has the Fourier series coefficients of the same rectangular pulse with a given period and a given time shift. We use the expression for the Fourier series coefficients of the rectangular pulse train to calculate the third dimension of space-frequency dictionaries.

B. Dictionary-based Sparse Representation Framework

The Fourier series coefficients of the underlying modulation $m(x, y, t)$ can be expressed as:

$$\mathbf{c}_l(c, y) = \frac{1}{T} \int_{<T>} m(x, y, t) e^{-ilw_0 t}\, dt. \tag{5}$$

where l corresponds to harmonics number.

The sparse representation in space-frequency is expressed as:

$$\mathbf{c} = \Phi \boldsymbol{\eta}, \tag{6}$$

where $\mathbf{c}$ is a vectorized form of Fourier series coefficients for all scan positions, Φ is the predetermined space-frequency dictionary and $\boldsymbol{\eta}$ is the vector of representation coefficients.

Then, our sparse space-frequency dictionary-based reconstruction problem can be formulated as follows:

$$\hat{\boldsymbol{\eta}}_w = \arg\min_{\boldsymbol{\eta}} \sum_{j=1}^{N} \|\mathbf{d}^j - H^j \Phi \boldsymbol{\eta}\|_2^2 + \lambda \|\boldsymbol{\eta}\|_1, \tag{7}$$

where j indicates the polarization direction for the linearly polarized illumination, N is the number of polarization directions corresponding to the number of observations, H^j is the Toeplitz matrix that implements convolution as a matrix operation. The optimization problem in Eq. 7 is solved using the quasi-Newton method explained in detail in [4], [7].

IV. Sparse Representation Results for Simulated LVI data

Our goal in this section is to test the performance of the proposed framework in a controlled experiment. Therefore, we designed an experiment where simulated LVI data of an inverter is created using a simulated PSF of a high NA subsurface imaging system and the CAD layout of an inverter designed in $32nm$ process node (see Fig. 2(a)). The simulated PSF for a linearly-polarized illumination with $x-$polarization is shown in Fig. 3. For $y-$polarization, we rotate the PSF by $90°$. The elliptical support provides higher resolution in one direction. There are 8 rectangular regions where modulations are observed when the device is operational. These correspond to various the gate and drain regions, shown in Fig. 2(b). For each of these regions, the amplitude of modulations is calculated as explained in Section II using a nominal voltage of $1V$, doping concentration of diffusion layers as $2e20$ and doping concentration of inversion channel as $9.15e16$. The calculated thicknesses and refractive indices for different layers around gate and drain regions when the transistor is in cut off regime and in linear operation region are as follows: $n_{poly} = 3.392, n_{ox} = 1.45, n_{channel} = 3.504 + 2.51j, n_{SCRoff} = 3.6, n_{SCRon} = 3.6, n_{diff} = 3.35, t_{poly} = 70, t_{ox} = 1.65, t_{channel} = 15, t_{SCRoff} = 50, t_{SCRon} = 80, t_{diff} = 40$. We have used the first five harmonics and created multiple harmonics LVI data. The amplitude and phase of the first harmonic for the observation with $x-$polarization illumination are shown in Figs. 4(a) and 4(b). The amplitude and phase of the first harmonic for the ground truth are shown in Figs. 4(c) and 4(d). The modulations in the gate regions are stronger than the modulations in drain regions. We performed reconstruction using both $x-$polarization and $y-$polarization data. The amplitude and phase of the first harmonic for the sparse reconstruction result are shown in Fig. 5. The sparse reconstruction was able to recover gate and drain regions which were blurred and merged in observations. Hence, the sparse representation framework increases the resolution and localization accuracy.

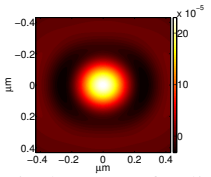

Fig. 3: PSF of the optical system for linearly-polarized input light in $x-$direction

In order to assess localization accuracy, we clustered scan positions into 3 different regions with different time behavior: no modulation (non-active regions), rectangular pulse with phase 0 and rectangular pulse with phase π. In order to represent the observation data and the reconstruction in time domain, we used Fourier series expansion in terms of the first five harmonics and then we applied K-means clustering [12]. The underlying true clusters are shown in Fig. 6(a). The clustering results for LVI data in $x-$polarization are shown in Figs. 6(b). The clustering results for sparse reconstruction are given in Fig. 7. We also calculated a localization accuracy metric defined as the number of scan positions with wrong cluster label divided by the total number of scan positions. Table I compares the localization accuracy for LVI observation data and sparse reconstruction. The localization accuracy of sparse reconstruction is significantly higher than the localization accuracy of LVI observation data.

Additionally, we simulated LVI data for a case when there is a stuck-at fault (stuck-at 0/1). For this case, no modulation will be observed underneath the drain regions but there will

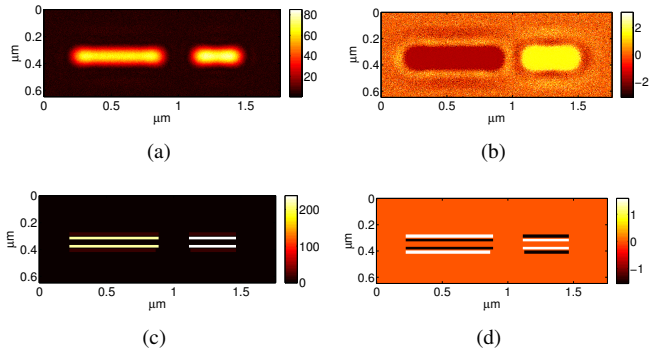

Fig. 4: (a)Amplitude and (b) phase of the 1st harmonic for LVI data with linearly-polarized input light in $x-$direction, (c) amplitude and (d) phase of the 1st harmonic for ground truth data

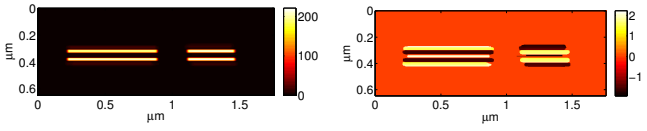

(a) (b)

Fig. 5: (a)Amplitude and (b) phase of the 1st harmonic for dictionary-based sparse representation result

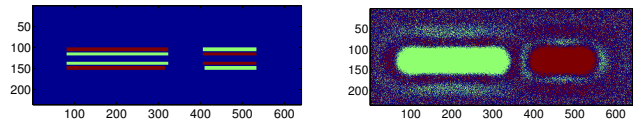

(a) (b)

Fig. 6: (a)True cluster labels and (b) cluster labels for LVI data with linearly-polarized input light in $x-$direction

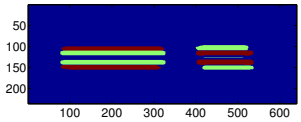

Fig. 7: Cluster labels for dictionary-based sparse reconstruction

Observation$-x$	Observation$-y$	Reconstruction
0.5043	0.3604	0.0341

TABLE I: Localization error in percent

be modulations underneath the gate regions. The amplitude and phase of the first harmonic for the observation with $x-$polarization illumination are shown in Fig. 8 and for the sparse reconstruction result in Fig. 9. The comparison of the LVI data for regular operation case and for stuck-at-fault case in Figs. 4 and 8, shows that because of the resolution limitation the fault cannot be detected in the observation data, as no changes are observed in the LVI data. However, the sparse representation results in Fig. 9 shows no modulation underneath drain regions whereas modulations are observed for regular operation in Fig. 5. Dictionary-based sparse reconstruction thus enables the localization of a stuck-at fault by providing resolution improvement.

V. Conclusion

In this work, a sparse space-frequency representation based on overcomplete dictionaries was proposed in order to increase spatial resolution and localization accuracy of LVI measurements. The proposed framework was validated on simulated data. IC imaging is particularly suitable for dictionary-based image reconstruction methods because the data is highly structured both spatially and temporally. An overcomplete dictionary, which can be predetermined using this structure, poses strong structural priors and enables recovery of high-frequency information. Scan positions can be accurately clustered into regions with different time behavior using the reconstruction results. However, clustering results using only LVI measurements do not produce accurate cluster labels. Simulations were performed for a regular operation case and a stuck-at-fault case. Reconstruction results for both scenarios show that dictionary-based sparse representation enables detection of the faults which are not detectable in blurry observation

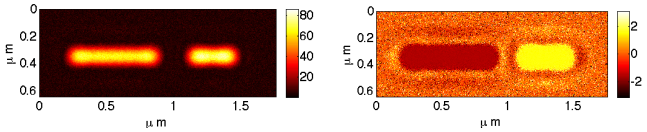

(a) (b)

Fig. 8: (a)Amplitude and (b) phase of the 1st harmonic for LVI data with linearly-polarized input light in $x-$direction for stuck-at-fault case

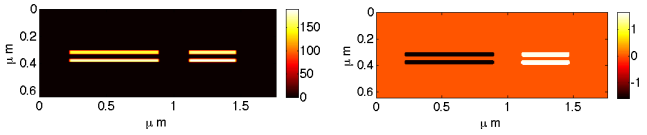

(a) (b)

Fig. 9: (a)Amplitude and (b) phase of the 1st harmonic for dictionary-based sparse representation result for stuck-at-fault case

data. More than 80% reduction in localization error has been shown.

Acknowledgment

This work was supported by IARPA via AFRL contract number: FA8650-11-C- 7102.

References

[1] F. H. Köklü *et al.*, "Subsurface microscopy of integrated circuits with angular spectrum and polarization control," *Opt. Lett.*, vol. 34, no. 8, pp. 1261–1263, Apr 2009.

[2] A. Yurt, *et al.*, "Effect of vector asymmetry of radially polarized beams in solid immersion microscopy," *Opt. Express*, vol. 22, no. 6, pp. 7320–7329, Mar 2014.

[3] A. Tuysuzoglu, *et al.*, "Sparsity driven ultrasound imaging," *The Journal of the Acoustical Society of America*, vol. 131, no. 2, pp. 1271–1281, 2012.

[4] M. Çetin and W. Karl, "Feature-enhanced synthetic aperture radar image formation based on nonquadratic regularization," *IEEE Transactions on Image Processing*, vol. 10, no. 4, pp. 623 –631, apr 2001.

[5] S. Gazit, *et al.*, "Super-resolution and reconstruction of sparse sub-wavelength images," *Opt. Express*, vol. 17, no. 26, pp. 23 920–23 946, Dec 2009.

[6] T. B. Cilingiroglu, *et al.*, "Image reconstruction techniques for high numerical aperture integrated circuit imaging," in *ISTFA*, Nov. 2012, pp. 551–556.

[7] T. Cilingiroglu, *et al.*, "Dictionary based image enhancement for integrated circuit imaging," in *ICASSP*, May 2013, pp. 1869–1873.

[8] Y. S. Ng *et al.*, "Laser voltage imaging: A new perspective of laser voltage probing," in *ISTFA*. ASM International, 2010.

[9] U. Kindereit, "Investigation of laser-beam modulations induced by the operation of electronic devices," Ph.D. dissertation, Berlin Institute of Technology, Berlin, Germany, 2009.

[10] D. L. Donoho and I. M. Johnstone, "Ideal spatial adaptation by wavelet shrinkage," *Biometrika*, vol. 81, pp. 425–455, 1994.

[11] S. Samadi *et al.*, "Multiple feature-enhanced synthetic aperture radar imagery," in *Algorithms for Synthetic Aperture Radar Imagery*, vol. 7337. SPIE, 2009, pp. 733 701–733 701.

[12] H. Späth, *Cluster dissection and analysis: theory, FORTRAN programs, examples*, ser. Computers and their applications. Horwood, 1985.